energies

MDPI

Article

A Comparative Life Cycle Assessment of Linear Free-Piston and Conventional Engines for Stationary and Automotive Applications

Andrea Di Mario [1], Antonella Accardo [1,*], Carlo Beatrice [2] and Ezio Spessa [1,*]

[1] Department of Energy "Galileo Ferraris" (DENERG), Politecnico di Torino, Corso Duca degli Abruzzi, 24, 10129 Turin, Italy; andrea.dimario@polito.it

[2] National Research Council—Institute of Sciences and Technologies for Sustainable Energy and Mobility (CNR-STEMS), 80125 Naples, Italy; carlo.beatrice@stems.cnr.it

* Correspondence: antonella.accardo@polito.it (A.A.); ezio.spessa@polito.it (E.S.)

Abstract

This study presents a Life Cycle Assessment (LCA) conducted to evaluate the environmental performance of a Free-Piston Linear Generator (FPLG) compared to conventional internal combustion engines in two applications: automotive range extenders and stationary generator sets. A cradle-to-grave approach was adopted, covering production, use, and end-of-life phases, with consistent modelling of engine materials, fuel supply chains (gasoline, diesel, hydrogen), and mission profiles. The FPLG, modelled based on key components (e.g., stator, magnets, coils), was evaluated under multiple hydrogen-production pathways, including steam methane reforming, wind- and photovoltaic-powered electrolysis, nuclear-based hydrogen production, and coal gasification. Conventional engine baselines were assessed using gasoline, diesel, and hydrogen pathways. Results highlight that environmental impacts are strongly driven by the fuel supply chain, particularly the Well-to-Tank phase. When hydrogen is produced through wind-powered electrolysis, the FPLG achieves over 90% reduction in fossil fuel consumption and more than 80% reduction in greenhouse gas emissions compared to gasoline. With hydrogen produced through steam methane reforming, benefits are limited in automotive applications but remain significant for stationary systems (>20% reduction in greenhouse gas emissions). However, hydrogen produced through wind-powered electrolysis increases impacts in categories such as resource use and toxicity due to materials and infrastructure required for wind farms and electrolyzers. The extended pathway analysis further showed that nuclear-based hydrogen achieved the lowest global warming potential among the investigated hydrogen scenarios, whereas coal gasification produced the highest climate-change impacts. These results confirm that the environmental performance of hydrogen-fuelled FPLG systems depends strongly on the upstream hydrogen-production pathway.

Keywords: free piston; hydrogen; LCA; sustainability; range extender; generator set

Academic Editors: Viktoria Mannheim, Patrycja Walichnowska and Weronika Kruszelnicka

Received: 4 August 2026
Revised: 3 September 2026
Accepted: 10 September 2026
Published: 15 September 2026

1. Introduction

In recent years, increasing attention has been directed toward free-piston linear generator (FPLG) technologies because of their potential for efficient and fuel-flexible electrical power generation in both automotive range-extender and distributed power-generation applications [1–3]. The environmental performance of road-vehicle and stationary power-generation technologies should be evaluated across the complete life cycle rather than solely on the basis of tailpipe or exhaust-stack emissions [4–6]. Road transport is a major component of global transport emissions: in 2019, direct greenhouse-gas emissions from transport were estimated at 8.7 Gt CO_2-eq, with road vehicles accounting for approximately 70% of direct transport emissions [7]. In parallel, stationary generator sets continue to be used as standby systems during grid outages and as electricity sources in off-grid applications [8,9]. For fuel-based power systems, life-cycle environmental performance is strongly influenced by upstream fuel production, processing, transport, and storage, in addition to the efficiency of the energy-conversion system [6,10]. Life Cycle Assessment (LCA), standardized by ISO 14040 and ISO 14044, therefore provides a consistent framework for comparing production, operation, and end-of-life burdens across alternative engine technologies [4,5]. More broadly, the transition toward environmentally sustainable propulsion has promoted the development of alternative drive systems based on electricity, hydrogen, and other alternative energy carriers, with the aim of reducing dependence on conventional fossil fuels and their associated environmental impacts [11]. Hydrogen-fuelled internal combustion engines (ICEs) have regained attention as a potential transition technology for decarbonizing combustion-based power systems. Their development can build on conventional piston-engine architectures, although hydrogen operation introduces specific challenges related to mixture formation, abnormal combustion, durability, and nitrogen oxides (NO_x) control [12]. However, hydrogen is not inherently low-carbon from a life-cycle perspective: hydrogen produced through unabated steam methane reforming (SMR) carries substantial upstream greenhouse-gas emissions, whereas electrolytic hydrogen can achieve substantially lower climate impacts only when the electricity supply is sufficiently low-carbon [6,10,13–15]. An automotive LCA of a hydrogen-fuelled engine reported substantial greenhouse-gas reductions when hydrogen was produced through wind-powered electrolysis; however, the magnitude of the benefit depended on the modelled hydrogen-production and fuel-supply pathways [16]. More broadly, hydrogen supply-chain assumptions and the selected system boundaries can materially affect comparative LCA results [6,10]. This dependence complicates comparisons across published LCA studies, since differences in functional units, background datasets, electricity mixes, hydrogen-production routes, technology maturity, and end-of-life assumptions may lead to substantially different results even for conceptually similar systems. Consequently, comparative assessments of hydrogen-fuelled ICEs, fossil-fuelled ICEs, and emerging engine-generator architectures should distinguish direct Tank-to-Wheel (TTW) or on-site emissions from upstream Well-to-Tank (WTT) impacts and from full cradle-to-grave results [4–6,13]. An FPLG is a crankless internal-combustion energy converter in which the reciprocating piston motion is coupled directly to a linear electrical machine, avoiding the intermediate conversion of piston motion into rotary shaft work [17–20]. The removal of the crankshaft and the associated slider-crank constraints means that the piston stroke, dead-centre positions, and compression ratio are determined by the interaction among combustion pressure, rebound forces, electromagnetic force, and moving-mass dynamics [17,18,20]. The absence of the crank mechanism can reduce mechanical losses, while the variable compression ratio can support fuel-flexible operation with different liquid and gaseous fuels [1,19]. A schematic representation of the FPLG architecture and its main functional components is shown in Figure 1.

These features also make the FPLG a tightly coupled multi-domain system, for which stable operation requires coordinated control of piston motion, combustion behaviour, and generator loading [20–24]. From an application perspective, FPLGs are particularly relevant when the required useful output is electricity rather than mechanical shaft work. In automotive powertrains, an FPLG can operate as a compact range extender for hybrid or extended-range electric vehicles, decoupling engine operation from wheel speed and allowing traction demand to be handled electrically [1,25,26]. In stationary applications, FPLGs have been investigated for distributed power generation and combined heat-and-power (CHP) configurations, where direct electricity generation, high efficiency, multi-fuel capability, and grid integration represent key technological requirements [2,3]. Within the present assessment, the two applications share the same conversion principle but are characterized by different functional units, operating profiles, service lives, and fuel-supply requirements. Despite the growing technical literature on FPLG architecture, combustion, linear electrical machines, control, and experimental validation [1–3,20,24], the life-cycle implications of replacing conventional engine-generator architectures with FPLGs remain insufficiently quantified. Available studies primarily address thermodynamic performance, piston dynamics, control strategies, linear-machine design, or component- and prototype-level validation rather than cradle-to-grave environmental performance. Consequently, the available literature provides detailed information on the technical performance and operating principles of free-piston systems, but offers limited evidence on whether these technological advantages translate into lower environmental impacts over the complete life cycle. In particular, differences in system boundaries, functional units, fuel-production assumptions, manufacturing inventories, and end-of-life modelling limit the possibility of directly comparing results obtained for different technologies and applications. A cradle-to-grave comparison should also include the production of FPLG-specific components, since their material and manufacturing requirements may shift part of the environmental burden from the use phase to the production phase [4,5]. This issue is particularly relevant for hydrogen scenarios. Renewable electrolytic hydrogen can substantially reduce life-cycle greenhouse-gas emissions relative to unabated fossil-based hydrogen [6,10,14,15]. However, the electricity and material requirements associated with electrolysis and renewable-power infrastructure may shift environmental burdens toward categories such as mineral resource depletion, human toxicity, and ecotoxicity [6,10,27]. The research problem addressed in this study is the lack of a harmonized life-cycle assessment capable of quantifying the environmental implications of introducing the free-piston architecture while comparing them with conventional architectures associated with the hydrogen, gasoline and diesel oil production pathways. This study addresses this gap through a harmonized cradle-to-grave comparative LCA of an FPLG and conventional engine baselines for two representative applications: an automotive range extender and a stationary generator set. The comparison adopts consistent system boundaries and harmonized assumptions for mission profiles, material inventories, service life, and end-of-life treatment, while evaluating gasoline, diesel, and alternative hydrogen supply pathways. By separating production, WTT, use-phase, and end-of-life contributions, the study identifies the conditions under which FPLGs can provide net life-cycle greenhouse-gas reductions, the extent to which these reductions depend on the hydrogen production route and application context, and the environmental trade-offs that must be considered beyond climate-change impacts. Based on the literature reviewed, no previous study was identified that simultaneously compares hydrogen-fuelled FPLGs and conventional engine-generator systems for both automotive and stationary applications using harmonized cradle-to-grave assumptions. The novelty of the present work therefore lies in combining these two application domains within a common life-cycle framework and in separately evaluating the influence of the engine architecture and the hydrogen-production pathway on the resulting environmental performance. By evaluating multiple hydrogen-production pathways together with different engine architectures, the study distinguishes the contribution of the energy carrier from that of the powertrain technology itself, providing a comprehensive assessment of the environmental trade-offs associated with free-piston systems. Accordingly, the study aims to (i) quantify the environmental performance of the hydrogen-fuelled free-piston technology relative to fossil- and hydrogen-fuelled conventional systems; (ii) distinguish the influence of the engine architecture from that of the hydrogen-production pathway; and (iii) identify the main life-cycle hotspots and environmental trade-offs associated with the investigated applications.

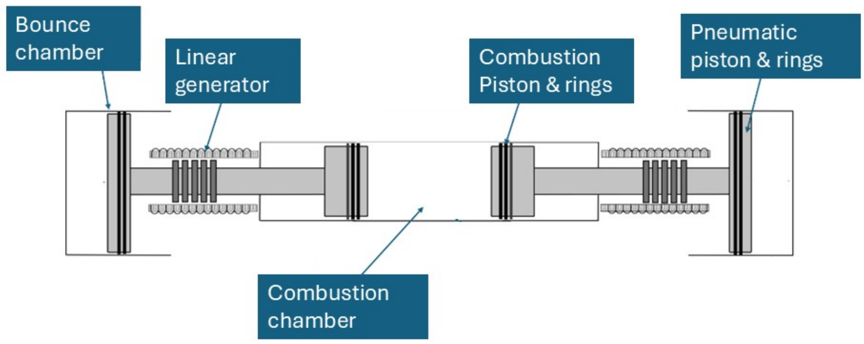

Figure 1. Schematic representation of the free-piston linear generator architecture, including the combustion chamber, linear generator, and pneumatic rebound system.

2. Materials and Methods

According to ISO 14040 and ISO 14044, LCA is a widely recognized methodology used to quantitatively assess the environmental impacts of a product or system over its entire life cycle, from raw material extraction to end-of-life treatment, including recycling or disposal [4,5]. All phases of this study were performed in accordance with ISO 14040 and ISO 14044, using SimaPro version 9.3.0.3 (PRé Sustainability B.V., Amersfoort, The Netherlands) for process modelling, inventory integration, impact assessment, and sensitivity analyses [28]. Background life-cycle data were obtained from the Ecoinvent 3.8 database (ecoinvent Association, Zurich, Switzerland) where database processes were required, while foreground data for the investigated engine configurations were derived from technical literature, manufacturer documentation, and engineering estimates as described in the following sections. SimaPro was selected because it enables the consistent integration of foreground inventory data with background life-cycle datasets within a common modelling environment, allowing the same impact assessment framework to be applied to all investigated configurations. ISO 14040 defines the principles and general framework of LCA, whereas ISO 14044 specifies the corresponding requirements and guidelines for goal and scope definition, inventory analysis, impact assessment, interpretation, and reporting. Their combined application provides the methodological basis for ensuring a transparent and consistent comparison among the investigated configurations. Following the standard framework, the LCA was structured into four interrelated phases. The goal and scope definition established the study objectives, system boundaries, functional unit, assumptions, and data limitations. The Life Cycle Inventory (LCI) phase quantified material and energy flows within the defined system, combining foreground modelling with background datasets and ensuring data quality and consistency. The Life Cycle Impact Assessment (LCIA) translated inventory results into environmental impact indicators using selected methods. Finally, the interpretation phase linked the results to the study objectives through hotspot identification and sensitivity analysis, supporting the interpretation of the comparative environmental performance. Compliance with ISO 14040 and ISO 14044 provides a standardized methodological framework but does not eliminate uncertainty associated with study-specific choices, including system boundaries, inventory data quality, technology maturity, and scenario assumptions. These aspects therefore remain relevant to the interpretation of the results and are considered among the limitations of the present assessment.

2.1. Goal and Scope

The goal of this study is to evaluate the environmental performance of hydrogen-fuelled free-piston systems relative to conventional engine technologies in automotive and stationary applications. The assessment adopts a cradle-to-grave system boundary, as illustrated in Figure 2. This boundary was selected to capture potential shifts in environmental burdens among component production, upstream fuel supply, system operation, and end-of-life treatment, rather than limiting the comparison to direct operational emissions.

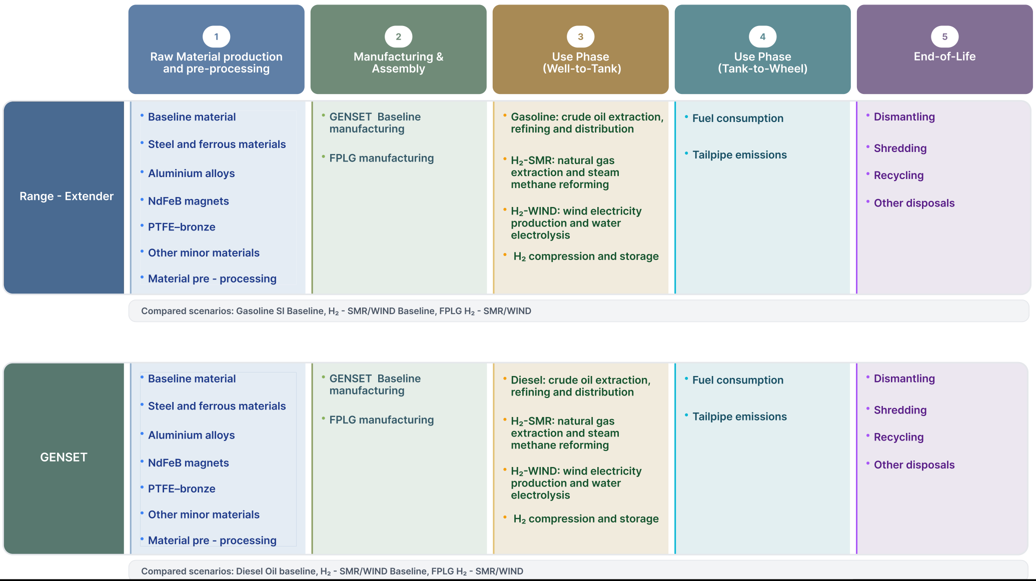

Figure 2. Cradle-to-grave system boundaries adopted for the automotive and stationary applications, including component production, fuel supply, system operation, and end-of-life stages.

The comparative assessment was structured across two application domains: automotive range extender and stationary genset, as summarized in Table 1. For each application, three configurations were analyzed: a conventional fossil-fuelled baseline (gasoline for automotive, diesel for stationary), a hydrogen-fuelled internal combustion engine (H_2-ICE) baseline, and the free-piston system operating on hydrogen.

The reference comparison between the FPLG and the conventional hydrogen-fuelled engine configurations was performed using steam methane reforming and wind-powered electrolysis, thereby allowing the influence of the conversion architecture to be assessed under equivalent hydrogen supply conditions.

To further investigate the influence of hydrogen production on the environmental performance of the FPLG, the hydrogen supply analysis was subsequently extended to three additional pathways: photovoltaic-powered electrolysis, nuclear-based hydrogen production, and coal gasification without carbon capture and storage. The FPLG configuration, conversion efficiency, material and manufacturing inventories, service life, functional unit, and end-of-life assumptions were maintained unchanged, while only the upstream hydrogen production inventory was modified. This extended scenario analysis therefore enables the influence of the hydrogen production route to be assessed independently of changes in the FPLG configuration.

This scenario setup enables a systematic comparison across both fuel types and engine technologies, ensuring methodological consistency and supporting a robust evaluation of the free-piston concept. While comparisons with fossil fuels can highlight the influence of lower-carbon fuel-production pathways, they may mask the specific contribution of the engine architecture. Therefore, hydrogen-based configurations are directly compared across different engine technologies (free-piston, spark-ignition, and compression-ignition), isolating the effect of the powertrain design from that of the fuel.

The main engine configurations and operating assumptions adopted for each scenario are summarized in Table 1.

Table 1. Main configurations and operating assumptions adopted for the comparative assessment.

Application	System/Reference	Fuel Pathway	Rated Power	Operating Parameter	Service Life	Functional Unit
Automotive range extender	MAHLE spark-ignition ICE	Gasoline	30 kW	BSFC > 250 g/kWh	240,000 km	1 km
	EVS H450-2 H_2-ICE	H_2-SMR / H_2-WIND	30 kW	BSFC 75–90 g H_2/kWh	240,000 km	1 km
	Sandia FPLG	H_2-SMR / H_2-WIND	30 kW	$\eta_e = 35.5\%$ BSFC 84.5 g H_2/kWh	240,000 km	1 km
Stationary genset	MB320 compression-ignition ICE	Diesel oil	330 kW	$\eta_{th} \approx 39\%$ BSFC 216 g/kWh	15,000 h	1 kWh
	Agenitor 412 H_2-ICE	H_2-SMR / H_2-WIND	330 kW	BSFC 80.9 g H_2/kWh	15,000 h	1 kWh
	Modular FPLG	H_2-SMR / H_2-WIND	330 kW	$\eta_e = 46.0\%$ BSFC 65.0 g H_2/kWh	15,000 h	1 kWh

2.2. Automotive Application—Range Extender

Three powertrain configurations were considered for the automotive application. The first is a free-piston engine prototype developed by Sandia National Laboratories (Albuquerque, NM, USA) [29], designed to deliver a nominal power of 30 kW in range-extender applications. The second is a conventional gasoline-fuelled range extender developed by MAHLE Powertrain Ltd. (Northampton, UK) Please check related highlights below [30], with an equivalent nominal power of 30 kW, used as the fossil-based baseline. The third configuration is a conventional hydrogen-fuelled range extender (H450-2) developed by EVS Hydrogen (Untergriesbach, Germany) [31], selected from publicly available technical documentation as a representative industrial solution for range-extender applications in the 15–25 kW range.

These configurations differ in both mechanical architecture and fuel type: the MAHLE engine operates on gasoline, whereas both the free-piston and the EVS engines are hydrogen-fuelled. This selection enables comparison across both fuel types and engine technologies, supporting a fair assessment of the free-piston concept relative to conventional alternatives.

For the free-piston engine, the bill of materials (BOM) data were taken from [29]. When data were unavailable, reasonable assumptions were adopted and, where necessary, parameters were estimated based on geometric considerations. Conservative choices were applied to ensure model consistency, transparency, and traceability. The main assumptions and equations are reported in the Supplementary Material.

For the gasoline baseline, the bill of materials was defined on the basis of the Ecoinvent dataset [32,33]. This dataset provides the Life Cycle Inventory for the production of an internal combustion engine for passenger car applications. The reference flow is one kilogram of engine produced and includes material flows, manufacturing processes, energy consumption, and process waste associated with the different production stages.

For the hydrogen baseline the Ecoinvent dataset [32], used previously for the gasoline range extender engine, was scaled based on the actual mass of the hydrogen engine in order to ensure a consistent comparison between the two architectures. More specifically, the structure of the process was kept unchanged, while the input flows were adjusted on the basis of the reference mass of the hydrogen-fuelled system. The main characteristics of the hydrogen engine selected as the baseline are [31]:

- model: H450-2, CHP/range-extender application (15–25 kW);
- total mass: 48 kg;

- maximum power at 3000 rpm: 30 kW.

For all engine configurations, including the free-piston system and baseline technologies, the use phase was modelled based on data from technical literature selected for technological relevance, methodological transparency, and availability of quantitative parameters. Consistent system boundaries were applied across all cases, encompassing fuel consumption, part-load efficiency, mission profiles, and emission factors. Where necessary, correction factors were introduced to harmonize differences in test cycles and operating conditions, ensuring comparability among the analyzed systems. The main assumptions and equations are reported in the Supplementary Material.

For the baseline configurations, the manufacturing inventory was included in the same Ecoinvent dataset used to derive the corresponding bill of materials. In contrast, the manufacturing processes of the free-piston engine were modelled on the basis of information available in the technical literature. For each component, a simplified transformation chain was defined, including casting, forging, machining from bar stock, sintering, lamination stamping, coil winding, and finishing operations. Each step was expressed both as a percentage of the finished component weight and as the associated material mass in kilograms. Wherever possible, the adopted values were derived from literature data on process yields, typical scrap rates, and raw material utilization levels. For cast components, reference was made to typical material yields reported for the main metallic materials [34]. For conventional machining operations, [35] was used as a methodological reference for the buy-to-fly concept and for the general magnitude of material losses associated with stock removal. However, since component-specific data were not available for the engine examined in this study, the values assigned to machining operations should be regarded as conservative engineering estimates. For powder metallurgy processes, a high raw material utilization rate was assumed, consistent with the values generally reported for near-net-shape technologies, typically above 95% [36]. For steel components produced by forging, the assumptions were based on general process information [37] and on literature data reporting flash losses in conventional hot forging in the range of 20% to 40% of the starting material [38]. For NdFeB magnets, the material losses associated with cutting, grinding, and polishing were derived from studies reporting scrap rates of approximately 30% of the raw material input. When expressed relative to the final magnet mass, this corresponds to a scrap incidence of approximately 43% [39]. For the stator core, a specific reference on the production of stator cores with concentrated windings was considered. The source reports iron scrap between 50% and 60% of the purchased material for 120 degree segments [40]. Since the masses in the present study were expressed relative to the finished component, this range corresponds to approximately 100% to 150% of the final lamination stack mass, depending on the ratio between purchased material and net output. For the copper windings, industrial evidence on EPS stators was considered, showing that winding scrap may range from approximately 30% to 0.1% under highly optimized conditions [41]. The adopted value of 5% was therefore selected as a conservative estimate within the reported range. Where directly transferable data were not available, including cutting losses from bar stock, non-intensive machining operations, and specific component geometries, conservative engineering estimates were introduced. These assumptions were kept distinct from the values directly supported by the literature in order to ensure transparency regarding data robustness and uncertainty. The assumptions adopted for each component are reported in Table 2.

https://doi.org/10.3390/en19184360

Table 2. Manufacturing assumptions adopted for the main free-piston engine components.

Component	Process Step	%	kg	Source
Piston, 7075-T6 aluminum [6.382 kg]	Al alloy casting feedstock, including gates and risers, yield ∼70%	143	9.13	[34]
	Finish machining	10	0.64	[35]
Compression rings, PTFE+bronze [0.070 kg]	Moulding/sintering, near-net-shape	5	0.004	[36]
	Ring finishing	10	0.007	[35]
Mover magnets, NdFeB [1.452 kg]	Pressing and sintering, negligible scrap	0	0.00	[36]
	Cutting, grinding and polishing	43	0.62	[39]
Aluminum spacers, Al 6061/7075 [0.052 kg]	Cutting from bar/extruded stock	5	0.003	estimate
	Spacer machining	30	0.016	[35]
Alternator, copper windings [2.630 kg]	Wire production, included in semi-finished product	0	0.00	–
	Coil winding and electrical connections	5	0.13	[41]
Combustion cylinder, AISI 4340 [9.685 kg]	Hot forging, including flash and process scrap	25	2.42	[37,38]
	Heavy machining	30	2.91	[35]
Rebound cylinder liner, AISI 4340 [21.416 kg]	Hot forging, including flash and process scrap	25	5.35	[37,38]
	Heavy machining	30	6.42	[35]
Back iron, 1018 steel [1.844 kg]	Cutting from bar/plate stock	5	0.09	estimate
	Machining	20	0.37	[35]
Stator, alloyed steel, laminations [31.294 kg]	Stamping of segmented laminations	122	38.25	[40]
	Stacking, welding/joining, negligible scrap	0	0.00	–

A consistent estimate of the use phase requires the definition of the specific fuel consumption of the engine. Although [29] provides the main reference data for the free-piston prototype, the reported performance values refer to an early-stage demonstrator and may not be fully representative of a more mature system. In particular, the conversion efficiency reported for the prototype is lower than that expected for an optimized free-piston architecture. Therefore, to avoid underestimating the potential environmental performance of the system, the specific hydrogen consumption was derived from [42], which reports an overall electrical efficiency of approximately 35.5%. This value was adopted as the reference efficiency in the present analysis.

The overall electrical efficiency is defined as the ratio between the net electrical output and the fuel energy input:

$$\eta_e = \frac{E_{\text{el}}}{E_{\text{fuel}}} \tag{1}$$

Accordingly, the specific hydrogen consumption, defined as the mass of hydrogen required to generate one unit of net electrical energy, was calculated as:

$$m^*_{\text{H}_2} = \frac{1}{\eta_e H_{i,\text{H}_2}} \tag{2}$$

where $m^*_{\text{H}_2}$ is expressed in $\text{kg}_{\text{H}_2}\,\text{kWh}^{-1}$.

For the gasoline baseline, technical data were required for a range extender system with a power output comparable to that of the SANDIA free-piston engine. The engine described in [43] was selected, as it provides performance data consistent with the reference operating conditions. These data were complemented with nameplate and configuration information from the MAHLE Powertrain datasheet [30]. The corresponding subsystem masses were used to define the bill of materials in Ecoinvent [32], scaling the datasets according to engine mass and ensuring consistency between production inventory and use phase modelling. According to [43], the selected operating point is characterized by:

- rotational speed: $n = 4000$ rpm;
- power output: $P \approx 30$ kW;
- brake specific fuel consumption: BSFC > 250 g kWh^{-1}.

The corresponding brake specific fuel consumption map is taken from [43].

Additional modelling data were derived from the manufacturer datasheet [30] to define subsystem masses, main engine specifications, and vehicle integration parameters. The document supported the reconstruction of the bill of materials and ensured consistency between the system boundaries adopted for the production inventory and the use phase analysis.

The specific fuel consumption of the hydrogen-fuelled range extender was considered in the range of 75 g kWh^{-1} to 90 g kWh^{-1}, based on the values reported in [31]. Applying the conversion procedure described in the Supplementary Material, the corresponding distance-based fuel consumptions are:

- 16.1 g km^{-1} @ 75 g kWh^{-1};
- 17.7 g km^{-1} @ 82.5 g kWh^{-1};
- 19.3 g km^{-1} @ 90 g kWh^{-1}.

In the present study, TTW emissions of the hydrogen-fuelled free-piston engine were assumed to be negligible for the reference case. This assumption does not imply that hydrogen internal combustion engines are intrinsically free of NOx emissions. Rather, it reflects the specific operating strategy considered for the analyzed FPLG, which is based on ultra-lean combustion, combustion phasing control, and low-temperature operation, conditions that are reported to substantially suppress thermal NOx formation [44].

Tailpipe carbon dioxide emissions from the gasoline baseline were estimated through a stoichiometric approach based on fuel consumption and average fuel composition detailed in Supplementary Material.

Tailpipe pollutants other than CO_2 were modelled by assuming that the gasoline baseline range extender, classified as an M1 spark-ignition vehicle, complies with Euro 6 limits. A conservative LCA approach was adopted by setting the main regulated pollutants equal to the corresponding limit values [45,46]. For particulate matter, the mass limit mainly applies to gasoline direct-injection systems. Since the final engine configuration was not defined, the most conservative value, 5 mg km^{-1}, was selected. The resulting TTW inputs were carbon monoxide (CO), total hydrocarbons (THC), non-methane hydrocarbons (NMHC), nitrogen oxides (NO_x), and particulate matter (PM), as reported in Table 3.

Table 3. Euro 6 emission limits adopted for the gasoline baseline [45,46].

Pollutant	Euro 6 Limit	Unit
CO	1.00	g/km
THC	0.10	g/km
NMHC	0.068	g/km
NO_x	0.06	g/km
PM (mass)	0.005	g/km

The WTT phase includes all upstream processes required to make the fuel available at the vehicle tank. It encompasses resource extraction, fuel production, processing, transport, distribution, and refuelling. For hydrogen pathways, the WTT assessment is particularly relevant because the associated environmental impacts depend strongly on the production technology, energy source, and infrastructure requirements. For the hydrogen-fuelled configurations, the WTT inventory associated with both SMR and wind-powered electrolysis pathways was derived from [47]. The corresponding WTT inventory for gasoline production and supply was modelled using the relevant Ecoinvent dataset [32].

Consistently with the bill of materials, the end-of-life (EoL) stage of both engines was modelled using an Ecoinvent dataset defined per unit mass [32]. The EoL stage was intended to represent current industrial waste-management practice for internal combustion engines rather than an optimized future circularity scenario specifically tailored to linear free piston engines. The engine is first shredded in a mechanical treatment facility, where direct emissions and emissions coming from electricity consumption are considered. Then, standard metallic fractions, such as aluminum and copper, were treated according to the corresponding mass-based Ecoinvent datasets, which include the conventional collection, sorting, recovery and recycling routes available in the database. The residue from the shredding is incinerated. No dedicated recovery of rare earth elements from NdFeB permanent magnets was included in the reference scenario. The exclusion of dedicated rare-earth recovery from NdFeB magnets should be interpreted as a conservative modelling choice.

2.3. Stationary Application—Genset

For the free-piston engine, a modular approach was adopted for the definition of the bill of materials. The stationary configuration was modelled as an assembly of eleven identical modules, each corresponding to a 30 kW free-piston unit, to achieve a total electrical output of 330 kW. This assumption enables direct scalability of the automotive configuration to the stationary application by leveraging the repeatability of the elementary module. Consequently, as a first-order approximation, the bill of materials of the stationary system is derived from that of the automotive case, with all engine-related components proportionally scaled by a factor of eleven.

For the hydrogen and diesel baseline genset, the bill of materials was based on [47].

However, the use-phase efficiency was not directly derived from the modular scaling of the automotive configuration. The overall efficiency of a stationary genset depends on the thermodynamic design, electrical architecture, auxiliary systems, and operating conditions of the complete system, which cannot be represented through a simple multiplication of the 30 kW module. Therefore, the reference electrical efficiency of the stationary free-piston genset was derived from [48], whereas the bill of materials and manufacturing inventory were based on the automotive configuration scaled by a factor of eleven.

For all engine configurations, including the free-piston system and baseline technologies, the use phase was modelled using data from technical literature selected for technological relevance, methodological transparency, and availability of quantitative parameters. Consistent system boundaries were applied across all cases, encompassing fuel consumption, efficiency at partial load, mission profiles, emission factors, and, where necessary, correction factors to harmonize differences in test cycles and operating conditions. This approach ensures comparability among the analyzed systems.

For the free-piston engine, the reference overall electrical efficiency was derived from [48]. The corresponding specific hydrogen consumption was combined with the nominal electrical power and the operating lifetime to determine the total hydrogen demand over the use phase. This quantity represents the total amount of hydrogen required by the stationary system throughout its operational life and was subsequently used to quantify the environmental impacts associated with the WTT and TTW stages.

For the hydrogen-fuelled baseline genset, the specific fuel consumption data were derived from the manufacturer datasheet [49]. The reference engine was assumed to operate with the same nominal power and operating lifetime adopted for the free-piston configuration, ensuring a consistent comparison between the two systems. The reported full-load hydrogen mass flow rate was converted into an energy-based specific hydrogen consumption, which represents the BSFC of the baseline engine under nominal operating conditions. This value was subsequently used to estimate the total hydrogen demand during the use phase and the associated WTT and TTW environmental impacts.

For the diesel reference genset, fuel consumption data were derived from the manufacturer datasheet [50]. The baseline system was modelled under the same nominal operating conditions and lifetime adopted for the free-piston configuration, ensuring consistency between the compared systems. Based on the reported fuel consumption and the lower heating value of diesel, the overall thermal efficiency was estimated at approximately 39%, which is consistent with the expected performance of a stationary diesel engine in this power range. The corresponding fuel consumption was used to estimate the total diesel demand during the use phase and the associated WTT and TTW environmental impacts.

For the TTW phase of the stationary application, three operating scenarios were defined to represent the configurations considered in the comparative assessment. The first scenario consists of a hydrogen-fuelled free-piston genset, evaluated using both SMR and WIND hydrogen pathways, consistently with the automotive case study. The second scenario represents a conventional hydrogen-fuelled genset, modelled using the same hydrogen supply routes to enable a direct comparison between the two system architectures under equivalent energy conditions. The third scenario consists of a diesel-fuelled conventional genset, representing the most mature and widely adopted technology for stationary power generation. This configuration was selected as the reference case for evaluating the environmental benefits associated with hydrogen use and the free-piston architecture.

For the hydrogen-fuelled gensets, the assumptions described for the automotive application were also applied to the stationary case. To ensure a consistent comparison across the different system architectures, TTW emissions were assumed to be zero for both hydrogen-fuelled configurations.

The TTW contribution of the baseline genset is not zero when the system is fuelled with diesel, as fuel combustion generates direct exhaust emissions. The diesel scenario therefore requires the explicit modelling of the main pollutants released during operation, including hydrocarbons (HC). The emission factors reported in Table 4 were derived from [47].

Table 4. TTW emission factors adopted for the diesel baseline genset.

Pollutant	Value	Unit
CO_2	3.55×10^4	g/h
CO	1.27×10^2	g/h
NO_x	6.01×10^1	g/h
HC	5.67×10^1	g/h
PM (mass)	1.73	g/h

For the estimation of carbon dioxide emissions, the stoichiometric approach described for the automotive application was also adopted for the stationary diesel baseline.

For the WTT phase, the modelling approach was consistent with that adopted for the automotive application, while accounting for the higher power demand and the corresponding operating profile of the stationary system.

For the stationary application, the EoL stage was modelled following the same approach adopted for the automotive case as described in Section 2.2.

2.4. Life Cycle Impact Assessment

The selected impact assessment method is the midpoint CML-IA baseline, as implemented in SimaPro. This method was selected because it provides a robust and widely adopted framework for comparing alternative energy systems while avoiding the additional modelling assumptions associated with endpoint methods. The objective of this study is not to aggregate environmental impacts into a single score, but rather to identify the dominant life-cycle hotspots associated with different fuel production pathways and propulsion technologies. Therefore, a midpoint-oriented impact assessment method was considered more appropriate than endpoint approaches. Furthermore, the selected impact categories, including climate change, fossil resource depletion, acidification, eutrophication, and toxicity, are particularly relevant for assessing hydrogen-based energy systems and are extensively used in previous LCA studies on internal combustion engines and hydrogen technologies [16].

In addition to the reference SMR and wind-powered electrolysis scenarios, an extended hydrogen-production pathway analysis was conducted for the FPLG. Three additional hydrogen supply routes were considered: photovoltaic-powered electrolysis, nuclear-based hydrogen production, and coal gasification without carbon capture and storage.

The analysis was performed independently for the automotive range extender and stationary genset applications. Within each application, the hydrogen demand and all FPLG-related modelling parameters were kept identical to the corresponding reference configuration. Therefore, the material inventory, manufacturing processes, conversion efficiency, operating lifetime, functional unit, and end-of-life treatment were not modified among hydrogen scenarios. Only the life-cycle inventory associated with hydrogen production and supply was changed.

This approach should be interpreted as a scenario analysis rather than as a parameter sensitivity analysis. The objective was to determine whether the environmental trends obtained from the original SMR and wind-powered electrolysis comparison remain valid when hydrogen is supplied through production routes characterized by substantially different upstream environmental profiles. All pathways were evaluated using the same CML-IA impact categories adopted for the reference assessment.

2.5. Sensitivity Analysis

A sensitivity analysis was conducted to evaluate the influence of the overall electrical conversion efficiency of the free piston on the life cycle global warming potential (GWP). Conversion efficiency was selected because it directly determines the specific hydrogen consumption and, consequently, the environmental burdens associated with hydrogen production and supply. All remaining inventory parameters, including rated power, operating load, service life, manufacturing requirements and end-of-life assumptions, were kept unchanged. The reference overall electrical efficiency was set to 35.5% for the automotive range extender, based on the free-piston linear configuration reported in [42]. For the stationary application, the reference efficiency was set to 46.0%, according to the performance reported by Mainspring Energy for its linear generator technology [48]. The lower and upper sensitivity cases were obtained by applying a relative variation of 10% to each reference value:

$$\eta_{\text{low}} = 0.90 \cdot \eta_{\text{ref}} \quad (3)$$

$$\eta_{\text{high}} = 1.10 \cdot \eta_{\text{ref}} \quad (4)$$

The resulting efficiency ranges were therefore 31.95–39.05% for the automotive range extender and 41.4–50.6% for the stationary genset. These lower and upper efficiencies represent sensitivity assumptions derived from the reference values and are not independent values taken from literature.

Since the brake specific fuel consumption is inversely proportional to conversion efficiency, the corresponding values were calculated as:

$$BSFC_i = BSFC_{\text{ref}} \cdot \frac{\eta_{\text{ref}}}{\eta_i} \quad (5)$$

where $BSFC_{\text{ref}}$ is the specific hydrogen consumption adopted in the reference inventory. The reference values were 84.5 g H_2/kWh for the automotive system and 65.0 g H_2/kWh for the stationary system. The percentage variation in GWP was calculated relative to the corresponding reference scenario as:

$$\Delta GWP_i = \frac{GWP_i - GWP_{\text{ref}}}{GWP_{\text{ref}}} \cdot 100 \quad (6)$$

To extend the sensitivity assessment beyond conversion efficiency, additional deterministic analyses were performed on selected material and manufacturing parameters of the FPLG.

For the material inventory, the stator and NdFeB permanent magnets were selected because they represent the two largest contributors to the GWP of the reference FPLG BOM, accounting for approximately 33.1% and 21.8%, respectively. A one-at-a-time approach was adopted, independently varying the mass of each component by ±20% relative to the reference inventory while keeping all other component masses and modelling parameters unchanged. The selected variation was used as a deterministic screening range to evaluate the influence of component-mass uncertainty and does not represent a probabilistic confidence interval.

Manufacturing uncertainty was assessed separately by varying the manufacturing requirements associated with the NdFeB permanent magnets. Magnet manufacturing was selected because it represents the largest contribution to the reference manufacturing-stage GWP, accounting for approximately 47.3% of the total manufacturing impact. The corresponding manufacturing inventory was varied by ±20%, while the material inventory and all other manufacturing processes were kept unchanged.

For both the component-mass and manufacturing analyses, the modified inventories were propagated through the complete cradle-to-grave models for the automotive range extender and stationary genset under both H_2 SMR and H_2 WIND pathways. Hydrogen consumption, conversion efficiency, service life, and end-of-life assumptions were kept unchanged. The percentage variation in each impact category was calculated relative to the corresponding reference scenario using the same formulation adopted for GWP.

The detailed calculations and complete sensitivity results for all impact categories are reported in the Supplementary Material.

Results of the sensitivity are shown in Section 3.2.

3. Results

3.1. Comparative Life Cycle Assessment

This section presents the comparative assessment of the full life cycle of the range extender configurations considered in the study. The analysis was structured as a Comparative Life Cycle Assessment, with all systems modelled using the same functional unit, mission profile, and system boundaries. The comparison is shown in Figure 3 with absolute values reported in Table 5. It includes the hydrogen-fuelled free-piston engine supplied with hydrogen produced through SMR and wind-powered electrolysis and the gasoline-fuelled spark-ignition baseline engine.

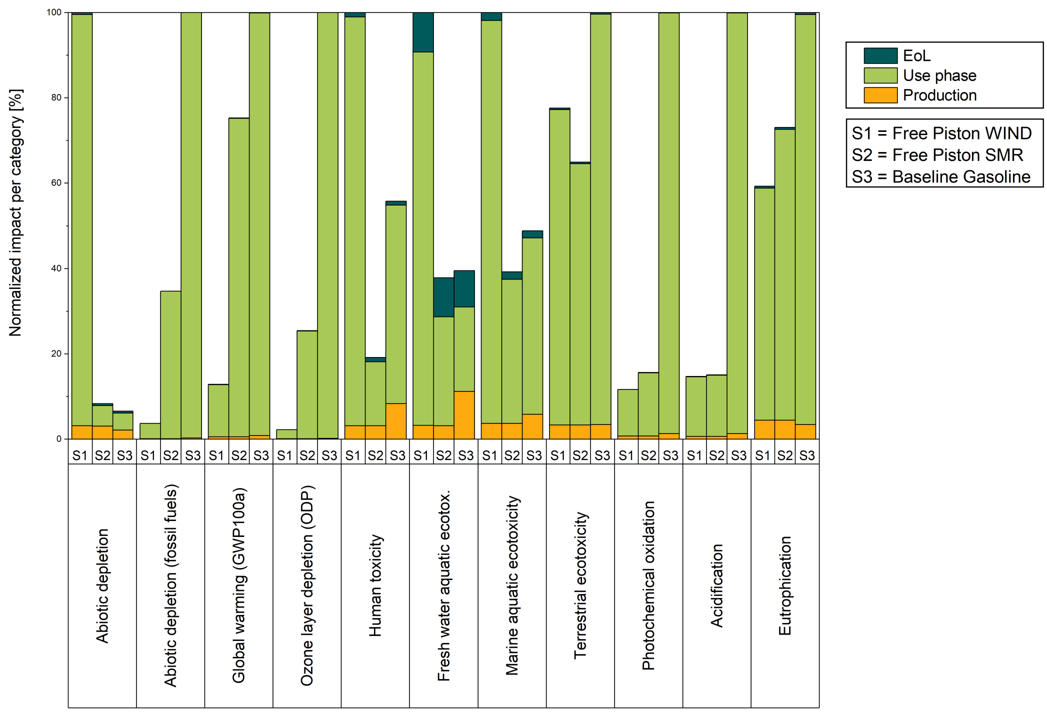

Figure 3. Comparative cradle-to-grave LCA results for the automotive range-extender configurations, including the hydrogen-fuelled FPLG supplied through SMR and wind-powered electrolysis and the gasoline spark-ignition baseline.

Table 5. Life cycle assessment results for the automotive configurations.

Impact Category	Unit	Free PISTON WIND	Free Piston SMR	Baseline Gasoline
Abiotic depletion	kg Sb eq	1.23	1.02×10^{-1}	8.10×10^{-2}
Abiotic depletion (fossil fuels)	MJ	1.11×10^{5}	1.04×10^{6}	3.00×10^{6}
Global warming (GWP100)	kg CO_2-eq	9.63×10^{3}	5.65×10^{4}	7.50×10^{4}
Ozone layer depletion (ODP)	kg CFC-11 eq	8.91×10^{-4}	9.98×10^{-3}	3.93×10^{-2}
Human toxicity	kg 1,4-DB eq	3.62×10^{4}	6.94×10^{3}	2.02×10^{4}
Fresh water aquatic ecotoxicity	kg 1,4-DB eq	3.01×10^{4}	1.14×10^{4}	1.19×10^{4}
Marine aquatic ecotoxicity	kg 1,4-DB eq	3.95×10^{7}	1.55×10^{7}	1.93×10^{7}
Terrestrial ecotoxicity	kg 1,4-DB eq	5.34×10^{1}	4.47×10^{1}	6.88×10^{1}
Photochemical oxidation	kg C_2H_4 eq	2.78	3.71	2.38×10^{1}
Acidification	kg SO_2 eq	5.76×10^{1}	5.90×10^{1}	3.92×10^{2}
Eutrophication	kg PO_4^{3-} eq	2.58×10^{1}	3.18×10^{1}	4.35×10^{1}

The gasoline baseline shows the highest impacts in the categories directly driven by fossil fuel production and combustion, including abiotic depletion of fossil resources, global warming, photochemical oxidation, acidification, and eutrophication. In this configuration, the WTT and TTW stages dominate the overall life cycle balance. The free-piston engine supplied with SMR hydrogen shows intermediate environmental performance. Although it reduces fossil resource use relative to the gasoline baseline, the dependence on natural gas limits the reduction in global warming and other energy-related impact categories. The free-piston engine supplied with WIND hydrogen provides the largest reduction in global warming and fossil abiotic depletion. However, this pathway increases impacts in abiotic depletion, human toxicity, freshwater aquatic ecotoxicity, and marine aquatic ecotoxicity, mainly due to the material requirements associated with renewable electricity infrastructure. Terrestrial ecotoxicity is also higher than in the SMR configuration, although it remains lower than in the gasoline baseline. In all configurations, the contribution of the engine bill of materials and manufacturing processes remains secondary compared with the fuel supply chain and use phase. Overall, the transition from the gasoline baseline to the hydrogen-fuelled free-piston engine is environmentally advantageous mainly when hydrogen is produced through renewable electricity. The main benefits concern climate change and fossil resource use, while the main trade-off is the increase in material-related toxicity and ecotoxicity impacts.

Figure 4 shows the comparison within the two hydrogen-fuelled configurations, with the absolute values reported in Table 6. It includes the LCA results for the free-piston engine and the baseline hydrogen-fuelled engine under different hydrogen-production pathways, namely SMR and wind-powered electrolysis.

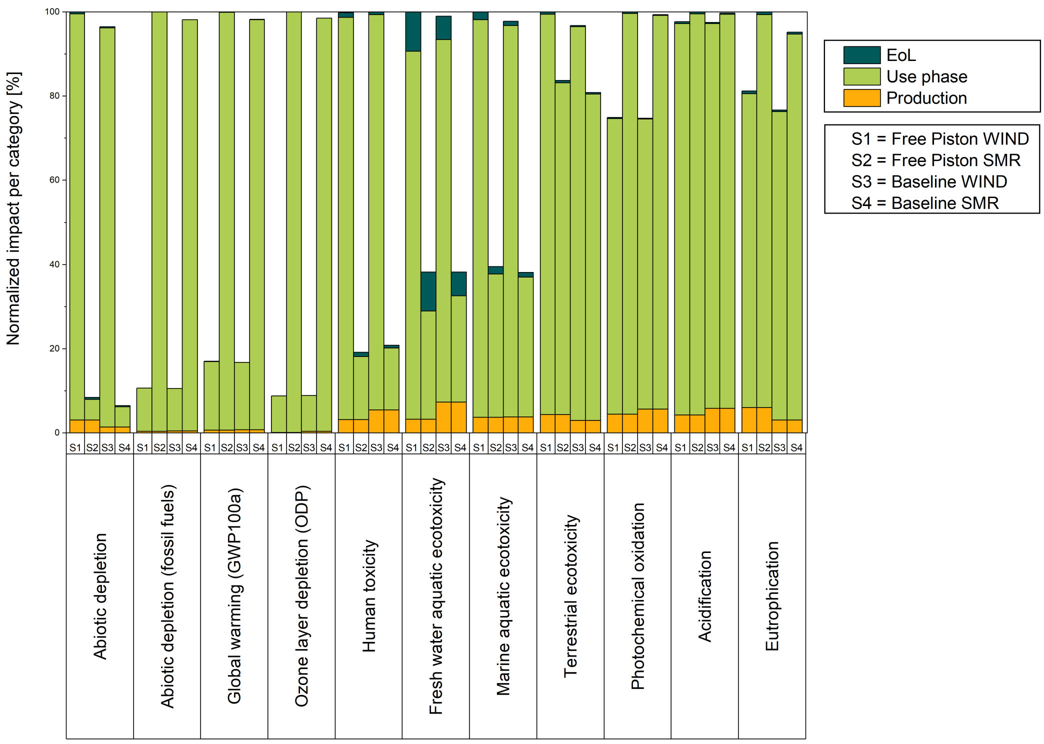

Figure 4. Comparative cradle-to-grave LCA results for the hydrogen-fuelled automotive range extenders, comparing the FPLG and conventional H_2-ICE under SMR and wind-powered electrolysis pathways.

The results indicate that the overall environmental profile is mainly driven by the hydrogen-production pathway, while the contributions of the engine BOM and EoL stage remain secondary. The two hydrogen pathways show opposite trends. The SMR pathway is more relevant in energy- and climate-related categories, including fossil depletion, global warming, ozone layer depletion, photochemical oxidation, acidification, and eutrophication. In contrast, the WIND pathway substantially reduces these impacts but increases non-fossil abiotic depletion, toxicity, and ecotoxicity impacts due to the material requirements associated with renewable electricity infrastructure. For a given hydrogen pathway, the differences between the free-piston engine and the conventional baseline remain limited in the overall life cycle balance. The higher efficiency of the free-piston configuration slightly reduces the WTT-related impacts; however, the hydrogen production route, whether SMR or WIND, remains the main driver of the total environmental performance.

Table 6. Life cycle assessment results for the two hydrogen-fuelled automotive configurations.

Impact Category	Unit	Free Piston WIND	Free Piston SMR	Baseline WIND	Baseline SMR
Abiotic depletion	kg Sb eq	1.20	1.01×10^{-1}	1.16	7.70×10^{-2}
Abiotic depletion (fossil fuels)	MJ	1.08×10^{5}	1.01×10^{6}	1.07×10^{5}	9.96×10^{5}
Global warming (GWP100a)	kg CO_2-eq	9.40×10^{3}	5.51×10^{4}	9.25×10^{3}	5.42×10^{4}
Ozone layer depletion (ODP)	kg CFC-11 eq	8.69×10^{-4}	9.72×10^{-3}	8.66×10^{-4}	9.57×10^{-3}
Human toxicity	kg 1,4-DB eq	3.53×10^{4}	6.80×10^{3}	3.55×10^{4}	7.39×10^{3}
Fresh water aquatic ecotoxicity	kg 1,4-DB eq	2.94×10^{4}	1.12×10^{4}	2.92×10^{4}	1.13×10^{4}
Marine aquatic ecotoxicity	kg 1,4-DB eq	3.85×10^{7}	1.52×10^{7}	3.77×10^{7}	1.48×10^{7}
Terrestrial ecotoxicity	kg 1,4-DB eq	5.21×10^{1}	4.36×10^{1}	5.05×10^{1}	4.21×10^{1}
Photochemical oxidation	kg C_2H_4 eq	2.72	3.62	2.71	3.60
Acidification	kg SO_2 eq	5.63×10^{1}	5.76×10^{1}	5.62×10^{1}	5.74×10^{1}
Eutrophication	kg PO_4^{3-} eq	2.52×10^{1}	3.11×10^{1}	2.38×10^{1}	2.96×10^{1}

Figure 5 compares four stationary configurations: the free-piston genset fuelled with hydrogen produced through SMR, the free-piston genset fuelled with hydrogen produced through wind-powered electrolysis, the conventional baseline genset fuelled with SMR-derived hydrogen, and the conventional baseline genset fuelled with hydrogen produced through wind-powered electrolysis. The corresponding absolute values are reported in Table 7.

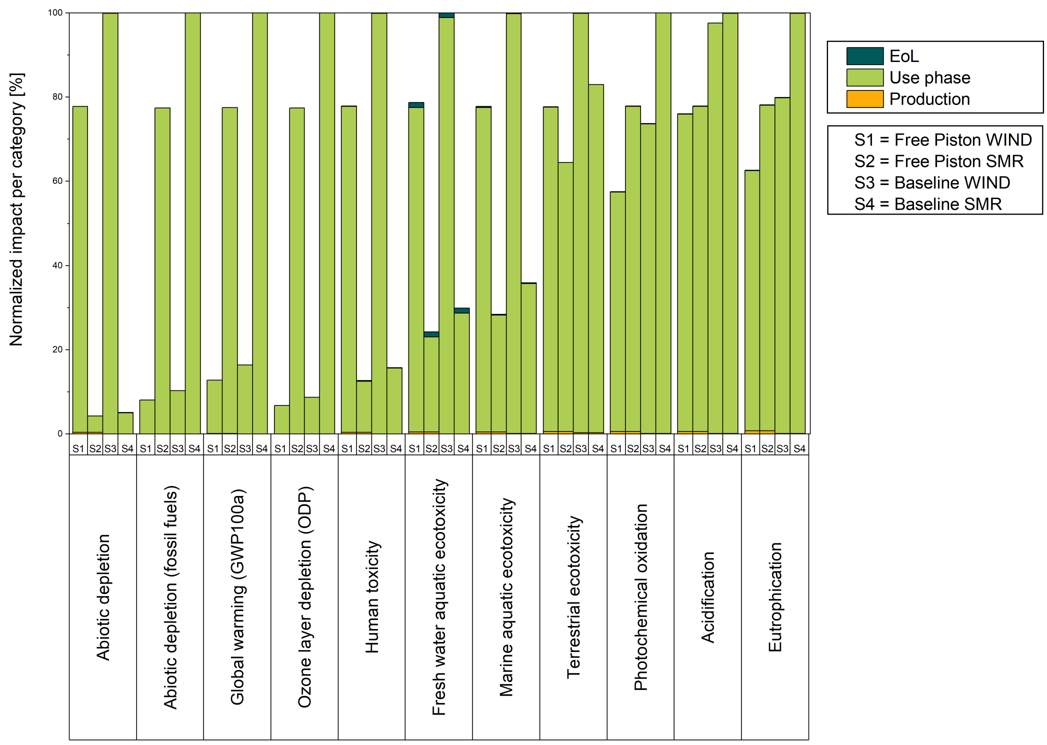

Figure 5. Comparative cradle-to-grave LCA results for the stationary hydrogen-fuelled gensets, comparing the FPLG and conventional H_2-ICE under SMR and wind-powered electrolysis pathways.

Table 7. Life cycle assessment results for the stationary hydrogen-fuelled scenarios.

Impact Category	Unit	Baseline WIND	Baseline SMR	Free Piston SMR	Free Piston WIND
Abiotic depletion	kg Sb eq	1.11×10^2	5.60	4.78	8.64×10^1
Abiotic depletion (fossil fuels)	MJ	1.00×10^7	9.70×10^7	7.51×10^7	7.80×10^6
Global warming (GWP100a)	kg CO_2-eq	8.63×10^5	5.26×10^6	4.08×10^6	6.72×10^5
Ozone layer depletion (ODP)	kg CFC-11 eq	8.11×10^{-2}	9.33×10^{-1}	7.22×10^{-1}	6.30×10^{-2}
Human toxicity	kg 1,4-DB eq	3.26×10^6	5.14×10^5	4.12×10^5	2.54×10^6
Fresh water aquatic ecotoxicity	kg 1,4-DB eq	2.49×10^6	7.43×10^5	6.03×10^5	1.96×10^6
Marine aquatic ecotoxicity	kg 1,4-DB eq	3.51×10^9	1.26×10^9	9.97×10^8	2.73×10^9
Terrestrial ecotoxicity	kg 1,4-DB eq	4.79×10^3	3.97×10^3	3.09×10^3	3.72×10^3
Photochemical oxidation	kg C_2H_4 eq	2.45×10^2	3.32×10^2	2.59×10^2	1.91×10^2
Acidification	kg SO_2 eq	5.16×10^3	5.28×10^3	4.11×10^3	4.02×10^3
Eutrophication	kg PO_4^{3-} eq	2.23×10^3	2.79×10^3	2.18×10^3	1.75×10^3

Overall, the stationary comparison indicates that the environmental performance of both genset configurations is mainly driven by the hydrogen-production pathway, while the contributions of the genset bill of materials and EoL stage remain limited, except in selected categories such as marine aquatic ecotoxicity. The SMR pathway shows the highest impacts in energy- and climate-related categories, including fossil resource depletion, global warming, photochemical oxidation, acidification, and eutrophication. Within this pathway, the free-piston configuration performs better than the conventional baseline due to its higher efficiency. The WIND pathway substantially reduces fossil resource use and greenhouse gas emissions. However, it introduces relevant impacts in categories associated with material use, toxicity, and ecotoxicity, including abiotic depletion of non-fossil resources, human toxicity, freshwater aquatic ecotoxicity, marine aquatic ecotoxicity, and terrestrial ecotoxicity. These impacts are mainly associated with the infrastructure required for renewable electricity generation. The results indicate that the transition from the conventional baseline to the free-piston architecture provides a consistent environmental improvement. However, the magnitude of this improvement remains lower than the effect associated with the selection of the hydrogen-production pathway. Therefore, the environmental performance of the stationary system cannot be evaluated on the basis of climate-related indicators alone, but requires a balanced assessment of the trade-offs associated with renewable energy infrastructure.

Figure 6 compares three stationary configurations: the free-piston genset fuelled with hydrogen produced through SMR, the free-piston genset fuelled with hydrogen produced through wind-powered electrolysis, and the diesel-fuelled conventional baseline genset. The corresponding absolute values are reported in Table 8.

To assess the robustness of the conclusions with respect to the hydrogen supply assumption, the FPLG was additionally evaluated using photovoltaic-powered electrolysis, nuclear-based hydrogen production, and coal gasification without carbon capture and storage. These scenarios were compared with the original SMR and wind-powered electrolysis cases while maintaining the FPLG configuration and hydrogen demand unchanged.

For the automotive application, the hydrogen-production pathway produced a pronounced effect on life-cycle GWP. Nuclear-based hydrogen resulted in the lowest value, approximately 4.69×10^3 kg CO_2-eq, followed by wind-powered electrolysis at approximately 9.40 × 10^3 kg CO_2-eq and photovoltaic-powered electrolysis at approximately 9.99 × 10^3 kg CO_2-eq. The corresponding value for SMR was approximately 5.51 × 10^4 kg CO_2-eq, whereas coal gasification resulted in approximately 1.04 × 10^5 kg CO_2-eq. For comparison, the gasoline baseline produced approximately 7.50 × 10^4 kg CO_2-eq.

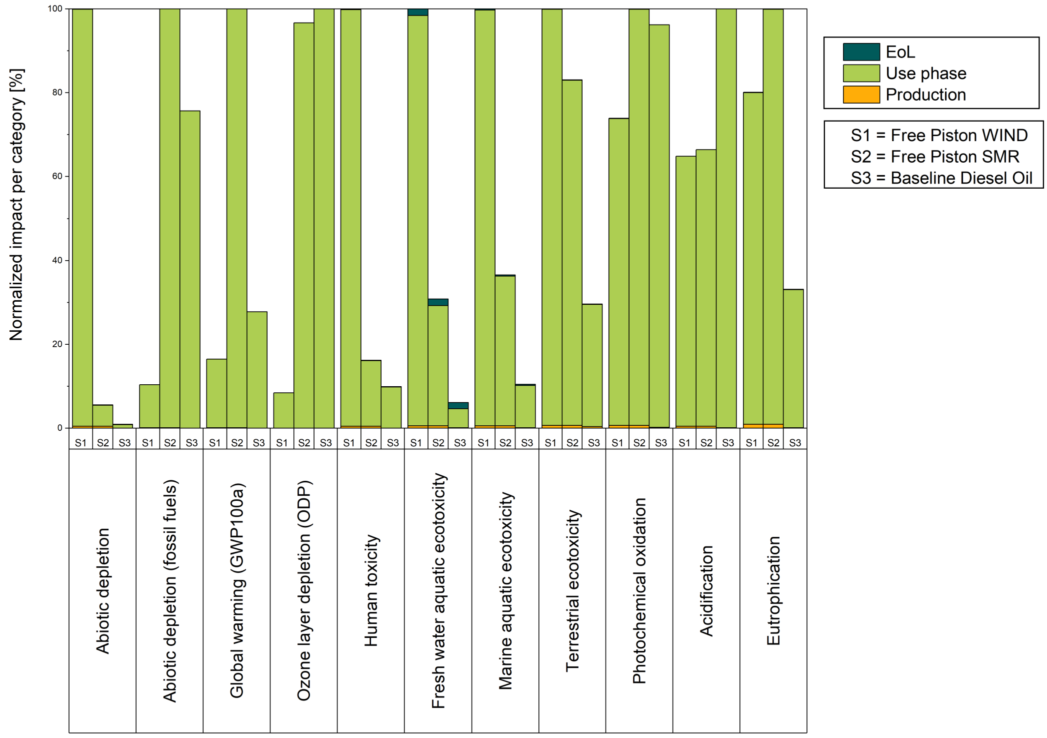

Figure 6. Comparative cradle-to-grave LCA results for the stationary FPLG supplied through SMR and wind-powered hydrogen pathways and the conventional diesel genset baseline.

Table 8. Life cycle assessment results for the stationary free-piston and diesel configurations.

Impact Category	Unit	Free Piston SMR	Free Piston WIND	Baseline Diesel
Abiotic depletion	kg Sb eq	4.78	8.64 × 10^1	7.91 × 10^{-1}
Abiotic depletion (fossil fuels)	MJ	7.51 × 10^7	7.80 × 10^6	5.68 × 10^7
Global warming (GWP100a)	kg CO_2-eq	4.08 × 10^6	6.72 × 10^5	5.98 × 10^5
Ozone layer depletion (ODP)	kg CFC-11 eq	7.22 × 10^{-1}	6.30 × 10^{-2}	7.47 × 10^{-1}
Human toxicity	kg 1,4-DB eq	4.12 × 10^5	2.54 × 10^6	2.52 × 10^5
Fresh water aquatic ecotoxicity	kg 1,4-DB eq	6.03 × 10^5	1.96 × 10^6	1.19 × 10^5
Marine aquatic ecotoxicity	kg 1,4-DB eq	9.97 × 10^8	2.73 × 10^9	2.86 × 10^8
Terrestrial ecotoxicity	kg 1,4-DB eq	3.09 × 10^3	3.72 × 10^3	1.10 × 10^3
Photochemical oxidation	kg C_2H_4 eq	2.59 × 10^2	1.91 × 10^2	2.49 × 10^2
Acidification	kg SO_2 eq	4.11 × 10^3	4.02 × 10^3	6.19 × 10^3
Eutrophication	kg PO_4^{3-} eq	2.18 × 10^3	1.75 × 10^3	7.22 × 10^2

The resulting automotive GWP ranking, from the lowest to the highest impact, was therefore nuclear-based hydrogen, wind-powered electrolysis, photovoltaic-powered electrolysis, SMR, gasoline, and coal gasification. Nuclear-based hydrogen reduced GWP by approximately 94% relative to the gasoline baseline, whereas hydrogen produced through coal gasification increased GWP by approximately 39%. This comparison demonstrates that the use of hydrogen does not intrinsically ensure a reduction in climate-change impacts, since the environmental benefit depends on the upstream production pathway.

The stationary application showed a similar dependence on hydrogen production, although the position of the conventional diesel baseline differed. Nuclear-based hydrogen resulted in approximately 3.19×10^5 kg CO_2-eq, compared with approximately 5.98×10^5 kg CO_2-eq for the diesel baseline, 6.72×10^5 kg CO_2-eq for wind-powered hydrogen, 7.14×10^5 kg CO_2-eq for photovoltaic-powered hydrogen, 4.08×10^6 kg CO_2-eq for SMR hydrogen, and 7.71×10^6 kg CO_2-eq for hydrogen produced through coal gasification.

The stationary GWP ranking was therefore nuclear-based hydrogen, diesel, wind-powered electrolysis, photovoltaic-powered electrolysis, SMR, and coal gasification. Nuclear-based hydrogen reduced GWP by approximately 47% relative to the diesel baseline. In contrast, wind- and photovoltaic-powered hydrogen showed GWP values approximately 12% and 19% higher than diesel, respectively, although both pathways substantially reduced fossil resource depletion. Coal gasification showed by far the highest climate-change impact among the investigated stationary scenarios.

The extended analysis also confirms that the GWP ranking cannot be generalized to all environmental impact categories. Nuclear-, wind-, and photovoltaic-based hydrogen substantially reduced climate-change and fossil-resource impacts relative to the more carbon-intensive hydrogen pathways, but higher impacts were observed in selected non-fossil resource depletion, toxicity, and ecotoxicity categories. Within the adopted inventories, nuclear-based hydrogen resulted in lower impacts than wind-powered hydrogen across the investigated CML-IA categories, whereas photovoltaic-powered hydrogen generally showed higher impacts than the corresponding wind-powered pathway.

Coal gasification produced a particularly unfavourable environmental profile, with high impacts not only for GWP but also for marine and terrestrial ecotoxicity, acidification, and eutrophication. Overall, these results strengthen the conclusion that hydrogen should not be treated as a uniform low-impact energy carrier in life-cycle assessments. The upstream production route can change both the magnitude and, in some cases, the direction of the environmental benefit relative to conventional fossil-fuel systems. The trends observed for the automotive application are consistent with previous life-cycle studies of hydrogen-based propulsion systems. Accardo et al. showed that the life-cycle greenhouse-gas performance of a hydrogen-fuelled internal combustion engine strongly depends on the hydrogen-production pathway, confirming the importance of accounting for upstream hydrogen production rather than considering only vehicle operation [16]. Similarly, Candelaresi et al. compared hydrogen-fuelled internal combustion, fuel-cell, and hybrid-electric passenger vehicles and identified wind-powered hydrogen as a favourable decarbonization option, while also highlighting the relevance of vehicle and infrastructure production to the overall environmental profile [51]. These findings are consistent with the present results, in which wind-powered electrolysis substantially reduces climate-change and fossil-resource impacts, while selected material-related toxicity, ecotoxicity, and resource-depletion impacts remain relevant. Direct comparison of absolute impact values should nevertheless be interpreted with caution because of differences in vehicle configurations, functional units, system boundaries, and background inventories among the studies. For stationary applications, the predominance of the operational and fuel-related stages is also consistent with previous life-cycle evidence. Benton et al. reported that the use phase accounted for more than 95% of the lifetime energy demand of a 455 kW standby diesel generator set, whereas the contributions associated with materials and manufacturing were substantially lower [52]. This trend is consistent with the present stationary assessment, in which fuel supply and operation dominate most impact categories, while the contributions of the genset bill of materials and end-of-life stage remain generally secondary. A systematic review of hydrogen-based power-generation LCAs by Rinawati et al. further showed that fuel cells are the most frequently investigated hydrogen conversion technology and that substantial methodological variability exists among published studies, particularly with respect to functional units, system boundaries, allocation procedures, and impact-assessment methods [53]. These methodological differences limit direct numerical comparison among studies. Moreover, no directly comparable cradle-to-grave LCA of a free-piston linear generator was identified in the literature reviewed for the present study, since published FPLG investigations remain predominantly focused on technical performance, system design, control, and experimental validation. The present results are therefore compared with previous studies primarily in terms of environmental trends and dominant life-cycle contributors rather than through direct benchmarking of absolute impact values.

From a practical implementation perspective, the environmental potential identified for the FPLG should be distinguished from its present technological and commercial readiness.

Compared with conventional reciprocating gensets, free-piston systems remain less mature in terms of long-term durability, control under variable operating conditions, manufacturing standardization, and large-scale deployment. Their commercialization therefore depends not only on conversion efficiency but also on reliable piston-motion control, component durability, system integration, and the development of a competitive manufacturing and maintenance chain [3,18,20].

For stationary applications, hydrogen-fuelled FPLGs may be particularly relevant in applications where hydrogen supply is already available or can be integrated with local low-carbon hydrogen production, such as distributed generation, backup power, or systems coupled with renewable electricity. However, large-scale deployment is constrained by hydrogen availability, storage requirements, transport and distribution infrastructure, and fuel cost. These constraints become particularly important when low-life-cycle-impact hydrogen is required, since the environmental advantage identified in the present study depends on the availability of a sufficiently low-impact hydrogen supply chain [14].

Consequently, hydrogen-fuelled stationary generators should not be interpreted as a universally scalable replacement for conventional gensets. Their suitability is expected to depend on the local energy system, operating profile, hydrogen-production pathway, and availability of storage and distribution infrastructure. A complete evaluation of commercial feasibility would additionally require capital cost, fuel cost, maintenance requirements, reliability, and infrastructure investment to be considered within a dedicated techno-economic assessment, which is outside the scope of the present LCA.

The present results should therefore be interpreted as an assessment of the environmental potential of the investigated configurations rather than as evidence of their immediate economic or commercial viability.

The results also indicate several potential mitigation strategies for reducing the life-cycle impacts associated with hydrogen supply.

For electrolytic hydrogen, the environmental performance is strongly dependent on the electricity used for hydrogen production. Increasing the share of low-impact renewable electricity and improving electrolyzer efficiency can reduce the electricity demand per unit of hydrogen produced and consequently lower the associated upstream burdens. At the same time, reductions in the material and energy requirements of renewable electricity and electrolysis infrastructure could limit the trade-offs observed in resource depletion, toxicity, and ecotoxicity categories.

Additional improvements may be achieved through reductions in the energy required for hydrogen compression, storage, transport, and distribution. Locating hydrogen production close to the point of use and improving storage and delivery efficiency may reduce these additional supply-chain burdens, although their relevance depends on the specific infrastructure configuration considered.

For fossil-based hydrogen pathways, substantial reductions in life-cycle greenhouse-gas emissions would require a decrease in the carbon intensity of hydrogen production itself. Therefore, improvements in the FPLG conversion system alone cannot compensate for a hydrogen supply chain characterized by high upstream environmental impacts.

These mitigation measures confirm that the environmental performance of hydrogen-fuelled FPLG systems depends on improvements across both the conversion technology and the hydrogen production and supply chain.

3.2. Results of the Uncertainty and Sensitivity Analysis

The discussion presented in this section focuses on GWP, while the complete sensitivity results for all impact categories are reported in the Supplementary Material. The GWP sensitivity results associated with the variation in overall electrical conversion efficiency are summarized in Table 9.

Table 9. Sensitivity of GWP results to the overall electrical conversion efficiency.

Application	Efficiency Variation	Efficiency [%]	BSFC [g H_2/kWh]	H_2 SMR		H_2 WIND	
				GWP [kg CO_2-eq]	Variation [%]	GWP [kg CO_2-eq]	Variation [%]
Range Extender	−10%	31.95	93.9	61,187	+11.03	10,391	+10.60
	Reference	35.50	84.5	55,108	0.00	9396	0.00
	+10%	39.05	76.8	50,143	−9.01	8583	−8.65
GENSET	−10%	41.40	72.2	4,527,593	+11.10	745,569	+11.03
	Reference	46.00	65.0	4,075,321	0.00	671,500	0.00
	+10%	50.60	59.1	3,705,281	−9.08	610,898	−9.02

For the automotive application, reducing the conversion efficiency by 10% increased the GWP by 11.03% under the H_2 SMR pathway and by 10.60% under the H_2 WIND pathway. The corresponding absolute increases were approximately 6079 kg CO_2-eq and 996 kg CO_2-eq over the assumed vehicle lifetime of 240,000 km. Increasing the efficiency by 10% reduced the GWP by 9.01% for H_2 SMR and by 8.65% for H_2 WIND, corresponding to avoided impacts of approximately 4965 kg CO_2-eq and 813 kg CO_2-eq, respectively. The slightly lower percentage sensitivity observed for the H_2 WIND automotive scenario indicates that a larger share of its total GWP is associated with contributions that remain constant when fuel consumption changes, including system production and end of life. Conversely, the H_2 SMR result follows the variation in hydrogen consumption more closely because the WTT contribution represents a larger share of the total climate change impact. For the stationary application, reducing the efficiency by 10% increased the GWP by 11.10% for H_2 SMR and by 11.03% for H_2 WIND. These variations correspond to absolute increases of approximately 452,272 kg CO_2-eq and 74,069 kg CO_2-eq over 15,000 operating hours. Increasing the efficiency by 10% reduced the GWP by 9.08% and 9.02%, avoiding approximately 370,040 kg CO_2-eq under the SMR pathway and 60,602 kg CO_2-eq under the WIND pathway. The larger absolute variations obtained for the stationary system result from its rated power of 330 kW and its extended operating lifetime. The close correspondence between fuel consumption and GWP variations also indicates that the stationary results are strongly dominated by the hydrogen supply phase. The asymmetric response of GWP to the two sensitivity directions is caused by the inverse relationship between efficiency and fuel consumption. A 10% reduction in efficiency increases hydrogen consumption by approximately 11%, whereas a 10% increase in efficiency reduces consumption by approximately 9%. The GWP results follow this relationship, particularly when the hydrogen-production pathway dominates the total life cycle impact. Although efficiency affects the GWP of both applications, the hydrogen-production pathway remains the main determinant of the absolute results. Under reference efficiency conditions, the GWP of H_2 SMR was approximately 5.9 times higher than that of H_2 WIND for the automotive application and 6.1 times higher for the stationary application. Therefore, an improvement in conversion efficiency produces a relevant reduction in climate change impacts, but it does not compensate for the higher carbon intensity associated with hydrogen produced from natural gas. The additional sensitivity analyses show that uncertainties associated with the FPLG material and manufacturing inventories have a substantially smaller influence on the cradle-to-grave results than conversion efficiency.

At the production-inventory level, a ±20% variation in stator mass resulted in a ±6.63% variation in the GWP of the FPLG BOM, while the same variation in NdFeB magnet mass resulted in a ±4.35% change. For the manufacturing inventory, the NdFeB magnet manufacturing processes accounted for approximately 47.3% of the reference manufacturing-stage GWP. Consequently, varying these manufacturing requirements by ±20% changed the manufacturing-stage GWP by approximately ±9.46%.

When these variations were propagated through the complete cradle-to-grave models, their relative influence was substantially reduced. The resulting GWP sensitivity for the automotive and stationary applications is summarized in Table 10. Detailed low, reference, and high results, together with the corresponding results for all CML-IA impact categories, are reported in the Supplementary Material.

Table 10. Summary of cradle-to-grave GWP sensitivity to component-mass and NdFeB manufacturing variations.

Application	Sensitivity Parameter	H_2 SMR GWP Variation [%]	H_2 WIND GWP Variation [%]
Range Extender	Stator mass ±20%	±0.0255	±0.1494
	NdFeB magnet mass ±20%	±0.0168	±0.0982
	NdFeB manufacturing ±20%	±0.0336	±0.1964
GENSET	Stator mass ±20%	±0.0038	±0.0231
	NdFeB magnet mass ±20%	±0.0025	±0.0152
	NdFeB manufacturing ±20%	±0.0050	±0.0303

For the automotive application, the largest GWP variation among the investigated production-related parameters was obtained for NdFeB manufacturing under the H_2 WIND pathway, with a variation of ±0.1964%. Under H_2 SMR, the corresponding variation was limited to ±0.0336%. The stator- and magnet-mass variations produced smaller effects, with maximum GWP changes of ±0.1494% and ±0.0982%, respectively.

For the stationary application, the relative influence was further reduced. The maximum GWP variation was ±0.0303% for NdFeB manufacturing under the H_2 WIND pathway, while all investigated production-related parameters resulted in variations below ±0.006% under H_2 SMR.

The complete impact-category results confirm that the response is category dependent. For stator-mass uncertainty, the maximum variation was approximately ±0.30%, observed for freshwater aquatic ecotoxicity in the automotive H_2 SMR scenario. For NdFeB magnet-mass uncertainty, the maximum variation was approximately ±0.43%, observed for eutrophication in the automotive H_2 WIND scenario. The manufacturing sensitivity showed the largest production-related response, with a maximum variation of approximately ±0.86% for eutrophication in the automotive H_2 WIND scenario. Nevertheless, all investigated component-mass and manufacturing variations remained below 1% when propagated through the complete life cycle.

The higher relative sensitivity generally observed for the H_2 WIND scenarios is associated with the lower contribution of hydrogen production to the total GWP. Consequently, production-related contributions represent a larger fraction of the overall impact than in the corresponding SMR scenarios, where upstream hydrogen production dominates the life-cycle result. Overall, the analysis confirms that the investigated BOM and manufacturing uncertainties affect the production inventory but do not materially alter the main cradle-to-grave conclusions of the study.

4. Conclusions

This study developed a cradle-to-grave comparative LCA of a hydrogen-fuelled linear free-piston engine and conventional engine technologies for automotive range extender and stationary genset applications. The results show that the environmental performance of the analyzed systems is mainly determined by the hydrogen-production pathway rather than by the engine architecture alone. In both applications, the WTT stage was the main contributor to the overall life cycle impacts, whereas the contributions of the engine BOM, manufacturing processes, and EoL stage were generally secondary, except in selected toxicity and ecotoxicity categories. For the automotive application, the extended hydrogen pathway analysis showed that nuclear-based hydrogen achieved the lowest GWP, followed by wind- and photovoltaic-powered electrolysis. SMR produced substantially higher climate-change impacts, whereas coal gasification resulted in a GWP higher than that of the gasoline baseline. The SMR pathway also improved the environmental performance, although to a lower extent because of its dependence on natural gas. However, the WIND pathway increased impacts related to non-fossil abiotic depletion, human toxicity, and freshwater and marine aquatic ecotoxicity, mainly due to the material requirements of renewable electricity generation and electrolysis infrastructure. A similar trend was observed for the stationary application. Among the extended hydrogen scenarios, nuclear-based hydrogen showed the lowest GWP and was the only investigated hydrogen pathway to achieve a lower GWP than the conventional diesel baseline. Wind- and photovoltaic-based hydrogen substantially reduced fossil resource depletion but resulted in slightly higher GWP than diesel, whereas SMR and coal gasification produced markedly higher climate-change impacts. Under the same hydrogen pathway, the free-piston genset performed better than the conventional hydrogen baseline because of its higher efficiency. However, the influence of the hydrogen production route was greater than the difference between the two engine architectures. Compared with the diesel baseline, hydrogen-based configurations showed lower impacts in selected climate-related and fossil resource categories when supplied with WIND hydrogen, while diesel remained competitive in some impact categories because of the upstream burdens associated with current hydrogen production systems.

The sensitivity analysis confirmed that conversion efficiency has a substantially greater influence on the cradle-to-grave results than the investigated uncertainties in component masses and manufacturing assumptions. A 10% reduction in efficiency increased GWP by approximately 10.6–11.1%, whereas a 10% improvement reduced it by approximately 8.7–9.1%, depending on the application and hydrogen-production pathway. In contrast, a $\pm$20% variation in the masses of the stator and NdFeB magnets produced maximum cradle-to-grave GWP variations of approximately $\pm$0.15% and $\pm$0.10%, respectively. A $\pm$20% variation in NdFeB manufacturing requirements resulted in a maximum GWP variation of approximately $\pm$0.20%. Across the complete set of impact categories, the largest production-related sensitivity was approximately $\pm$0.86%. These results indicate that the main comparative conclusions are robust with respect to the investigated BOM and manufacturing assumptions, while hydrogen production and conversion efficiency remain the dominant determinants of life-cycle environmental performance.

The extended hydrogen pathway analysis further confirms that the environmental performance of the FPLG cannot be attributed to hydrogen use alone. Among the investigated hydrogen production routes, nuclear-based hydrogen resulted in the lowest GWP for both applications, followed by wind- and photovoltaic-powered electrolysis, whereas steam methane reforming and particularly coal gasification produced substantially higher climate-change impacts. In the automotive application, coal-derived hydrogen resulted in a higher GWP than the gasoline baseline, while in the stationary application only nuclear-based hydrogen achieved a lower GWP than the diesel baseline. These results demonstrate that the environmental advantage of the FPLG depends on the complete life-cycle performance of the hydrogen production and supply chain and cannot be inferred from Tank-to-Wheel emissions alone. Furthermore, the ranking of hydrogen pathways was impact-category-dependent, since pathways characterized by low GWP and fossil-resource demand could present higher burdens in selected resource depletion, toxicity, and ecotoxicity categories. Future research should extend the scenario assessment to additional hydrogen production routes not considered in the present analysis, including biomass-derived hydrogen and CCS-assisted hydrogen production, provided that harmonized and sufficiently robust life-cycle inventories are available. Further work should also address prospective improvements in electricity generation, electrolysis, hydrogen transport and storage, primary manufacturing data, and validation of FPLG performance under representative operating conditions.

Supplementary Materials: The following supporting information can be downloaded at: https://www.mdpi.com/article/10.3390/en19184360/s1. Table S1. Free piston engine bill of materials. Table S2. Sensitivity of the automotive impact results to a relative variation of ±10% in the overall electrical conversion efficiency. Table S3. Sensitivity of the stationary genset impact results to a relative variation of ±10% in the overall electrical conversion efficiency. Table S4. Sensitivity of GWP results to the overall electrical conversion efficiency. Table S5. Sensitivity of cradle-to-grave GWP results to a ±20% variation in stator and NdFeB magnet mass. Table S6. Sensitivity of cradle-to-grave GWP results to a ±20% variation in NdFeB magnet manufacturing requirements.

Author Contributions: Conceptualization, A.A., C.B. and E.S.; methodology, A.A. and A.D.M.; software, A.A. and A.D.M.; investigation, A.A. and A.D.M.; data curation, A.A. and A.D.M.; writing—original draft preparation, A.A. and A.D.M.; writing—review and editing, A.A., C.B. and E.S.; supervision C.B. and E.S. All authors have read and agreed to the published version of the manuscript.

Funding: This research was funded by the Italian Ministry of University and Research (MUR) under the PRIN 2022 programme, grant number 2022988F33_PE8, within the project FLEXi-fuel high-efficiency linear piston engine for future power GENerators (FLEX-GEN).

Data Availability Statement: The raw data supporting the conclusions of this article will be made available by the authors on request. The data are not publicly available because some of the datasets are too large to be shared directly.

Acknowledgments: This work was performed at the interdepartmental Center for Automotive Research and Sustainable mobility (CARS).

Conflicts of Interest: The authors declare no conflicts of interest.

Abbreviations

The following abbreviations are used in this manuscript:

BOM	Bill of Materials
BSFC	Brake Specific Fuel Consumption
CFC	Chlorofluorocarbon
CHP	Combined Heat and Power
CLCA	Comparative Life Cycle Assessment
CML-IA	CML Impact Assessment method
CO	Carbon Monoxide

CO_2	Carbon Dioxide
DC	Direct Current
EoL	End of Life
FPLG	Free-Piston Linear Generator
GHG	Greenhouse Gas
GWP	Global Warming Potential
GWP100a	Global Warming Potential over a 100-year time horizon
H_2	Hydrogen
H_2-ICE	Hydrogen-fuelled Internal Combustion Engine
HC	Hydrocarbons
ICE	Internal Combustion Engine
ISO	International Organization for Standardization
LCA	Life Cycle Assessment
LCI	Life Cycle Inventory
LCIA	Life Cycle Impact Assessment
LHV	Lower Heating Value
M1	Passenger-car vehicle category
NMHC	Non-Methane Hydrocarbons
NO_x	Nitrogen Oxides
ODP	Ozone Depletion Potential
PM	Particulate Matter
SMR	Steam Methane Reforming
THC	Total Hydrocarbons
TTW	Tank-to-Wheel
WIND	Wind-powered electrolysis pathway
WTT	Well-to-Tank

References

1. Scopelliti, A.; Misul, D.A.; Santonocito, F.; Baratta, M. Optimization of Performance and Efficiency of a Fuel-Flexible Free-Piston Linear Generator (FPLG) Engine for Range Extender Application. *Energies* **2026**, *19*, 2064. [CrossRef]
2. Gianetti, G.G.; Morandi, N.; Lucchini, T.; Ferrarini, M.; Onorati, A. Towards 50% Efficiency in Opposed Free-Piston Linear Generators Operating with Natural Gas and HCCI Combustion. *Energies* **2026**, *19*, 2833. [CrossRef]
3. Famouri, P.; Subramanian, J.; Mahmudzadeh-Ghomi, F.; Bade, M.; Musho, T.; Clark, N. Development and Experimental Validation of a Tubular Permanent Magnet Linear Alternator for Free-Piston Engine Applications. *Machines* **2025**, *13*, 651. [CrossRef]
4. *ISO 14040:2021*; Environmental Management. Life Cycle Assessment. Principles and Framework; ISO: Geneva, Switzerland, 2021.
5. *ISO 14044:2021*; Environmental Management. Life Cycle Assessment. Requirements and Guidelines; ISO: Geneva, Switzerland, 2021.
6. Maniscalco, M.P.; Longo, S.; Cellura, M.; Miccichè, G.; Ferraro, M. Critical Review of Life Cycle Assessment of Hydrogen Production Pathways. *Environments* **2024**, *11*, 108. [CrossRef]
7. Intergovernmental Panel on Climate Change. (Ed.) *Climate Change 2022-Mitigation of Climate Change: Working Group III Contribution to the Sixth Assessment Report of the Intergovernmental Panel on Climate Change*, 1st ed.; Cambridge University Press: Cambridge, UK, 2023. [CrossRef]
8. Faraji, J.; Babaei, M.; Bayati, N.; Hejazi, M.A. A Comparative Study between Traditional Backup Generator Systems and Renewable Energy Based Microgrids for Power Resilience Enhancement of a Local Clinic. *Electronics* **2019**, *8*, 1485. [CrossRef]
9. Aris, A.; Shabani, B. Sustainable Power Supply Solutions for Off-Grid Base Stations. *Energies* **2015**, *8*, 10904–10941. [CrossRef]
10. Shaya, N.; Glöser-Chahoud, S. A Review of Life Cycle Assessment (LCA) Studies for Hydrogen Production Technologies through Water Electrolysis: Recent Advances. *Energies* **2024**, *17*, 3968. [CrossRef]
11. Milojević, S.; Skrucany, T.; Milošević, H.; Stanojević, D.; Pantić, M.; Stojanović, B. Alternative Drive Systems and Environmentally Friendly Public Passengers Transport. *Appl. Eng. Lett. J. Eng. Appl. Sci.* **2018**, *3*, 105–113. [CrossRef]
12. Stepien, Z. Analysis of the Challenges and Development of Hydrogen-Powered Combustion Piston Engines. *Energies* **2026**, *19*, 1898. [CrossRef]
13. Prussi, M.; Yugo, M.; De Prada, L.; Padella, M.; Edwards, R.; Lonza, L. *JEC Well-to-Tank Report V5: JEC Well to Wheels Analysis: Well to Wheels Analysis of Future Automotive Fuels and Powertrains in the European Context*; Publications Office of the European Union: Luxembourg, 2020. [CrossRef]

14. IEA. Global Hydrogen Review 2024–Analysis. 2024. Available online: https://www.iea.org/reports/global-hydrogen-review-2024 (accessed on 13 April 2026).
15. De Kleijne, K.; Huijbregts, M.A.J.; Knobloch, F.; Van Zelm, R.; Hilbers, J.P.; De Coninck, H.; Hanssen, S.V. Worldwide greenhouse gas emissions of green hydrogen production and transport. *Nat. Energy* **2024**, *9*, 1139–1152. [CrossRef]
16. Accardo, A.; Costantino, T.; Malagrinò, G.; Pensato, M.; Spessa, E. Greenhouse Gas Emissions of a Hydrogen Engine for Automotive Application through Life-Cycle Assessment. *Energies* **2024**, *17*, 2571. [CrossRef]
17. Mikalsen, R.; Roskilly, A. A review of free-piston engine history and applications. *Appl. Therm. Eng.* **2007**, *27*, 2339–2352. [CrossRef]
18. Hung, N.B.; Lim, O. A review of free-piston linear engines. *Appl. Energy* **2016**, *178*, 78–97. [CrossRef]
19. Woo, Y.; Lee, Y.J. Free piston engine generator: Technology review and an experimental evaluation with hydrogen fuel. *Int. J. Automot. Technol.* **2014**, *15*, 229–235. [CrossRef]
20. Wang, X.; Chen, F.; Zhu, R.; Yang, G.; Zhang, C. A Review of the Design and Control of Free-Piston Linear Generator. *Energies* **2018**, *11*, 2179. [CrossRef]
21. Mikalsen, R.; Roskilly, A. The control of a free-piston engine generator. Part 1: Fundamental analyses. *Appl. Energy* **2010**, *87*, 1273–1280. [CrossRef]
22. Mikalsen, R.; Roskilly, A. The control of a free-piston engine generator. Part 2: Engine dynamics and piston motion control. *Appl. Energy* **2010**, *87*, 1281–1287. [CrossRef]
23. Jia, B.; Mikalsen, R.; Smallbone, A.; Zuo, Z.; Feng, H.; Roskilly, A.P. Piston motion control of a free-piston engine generator: A new approach using cascade control. *Appl. Energy* **2016**, *179*, 1166–1175. [CrossRef]
24. Feng, H.; Song, Y.; Zuo, Z.; Shang, J.; Wang, Y.; Roskilly, A. Stable Operation and Electricity Generating Characteristics of a Single-Cylinder Free Piston Engine Linear Generator: Simulation and Experiments. *Energies* **2015**, *8*, 765–785. [CrossRef]
25. Smallbone, A.; Hanipah, M.R.; Jia, B.; Scott, T.; Heslop, J.; Towell, B.; Lawrence, C.; Roy, S.; Shivaprasad, K.V.; Roskilly, A.P. Realization of a Novel Free-Piston Engine Generator for Hybrid-Electric Vehicle Applications. *Energy Fuels* **2020**, *34*, 12926–12939. [CrossRef]
26. Jia, B.; Smallbone, A.; Zuo, Z.; Feng, H.; Roskilly, A.P. Design and simulation of a two- or four-stroke free-piston engine generator for range extender applications. *Energy Convers. Manag.* **2016**, *111*, 289–298. [CrossRef]
27. Mehmeti, A.; Angelis-Dimakis, A.; Arampatzis, G.; McPhail, S.J.; Ulgiati, S. Life Cycle Assessment and Water Footprint of Hydrogen Production Methods: From Conventional to Emerging Technologies. *Environments* **2018**, *5*, 24. [CrossRef]
28. PRé Sustainability. SimaPro. Available online: https://simapro.com/ (accessed on 10 November 2025).
29. Leick, M.T.; Moses, R.W. Experimental Evaluation of the Free Piston Engine - Linear Alternator (FPLA). Technical Report SAND2015–2095. 1177159, 569665, 2015. Available online: https://www.osti.gov/biblio/1177159 (accessed on 23 August 2025).
30. MAHLE Powertrain. MAHLE Compact Range Extender Engine-MAHLE Powertrain. Available online: https://www.mahle-powertrain.com/en/experience/mahle-compact-range-extender-engine/ (accessed on 23 August 2025).
31. EVS hydrogen GmbH. Hydrogen engine, 2025. Available online: https://www.evs-hydrogen.de/en/multifuel-engine-h2-ready (accessed on 23 September 2025).
32. Ecoinvent. Ecoinvent. Available online: https://ecoinvent.org/database/ (accessed on 23 September 2025).
33. Wernet, G.; Bauer, C.; Steubing, B.; Reinhard, J.; Moreno-Ruiz, E.; Weidema, B.P. The ecoinvent Database Version 3 (Part I): Overview and Methodology. *Int. J. Life Cycle Assess.* **2016**, *21*, 1218–1230. [CrossRef]
34. Joshi, D.; Modi, Y. Evaluating Environmental Impacts of Sand Cast Products Using Life Cycle Assessment. 2011. Available online: https://www.researchgate.net/publication/281810297_Evaluating_Environmental_Impacts_of_Sand_Cast_Products_Using_Life_Cycle_Assessment (accessed on 1 October 2025).
35. Nimbalkar, S.U.; Cox, D.; Visconti, K.; Cresko, J. Life Cycle Energy Assessment Methodology, Tool and Case Studies for Additive Manufacturing. Technical Report ORNL/TM–2014/93, Oak Ridge National Laboratory (ORNL), Oak Ridge, TN (United States), 2014. Available online: https://www.osti.gov/biblio/2406757 (accessed on 8 October 2025).
36. Dicoi, S.A. What Is Powder Metallurgy? Available online: https://dicoi-pm.com/en/what-is-powder-metallurgy/ (accessed on 16 September 2025).
37. Mulan Metal. Casting vs Forging Cost. 2025. Available online: https://www.mulanmetal.com/casting-vs-forging-cost/ (accessed on 8 August 2026).
38. Takemasu, T.; Vazquez, V.; Painter, B.; Altan, T. Investigation of metal flow and preform optimization in flashless forging of a connecting rod. *J. Mater. Process. Technol.* **1996**, *59*, 95–105. [CrossRef]
39. Wang, H.; Wang, J.; Lei, X.; Wen, X.; Li, D.; Liu, F.; Zhou, W.; Xu, S. Separation and Recovery of Rare Earths and Iron from NdFeB Magnet Scraps. *Processes* **2023**, *11*, 2895. [CrossRef]
40. Libert, F.; Soulard, J. *Manufacturing Methods of Stator Cores with Concentrated Windings*; IET: Stevenage, UK, 2006.
41. Nystator. Stator Bonding Manufacturer–Axial Flux Stator. 2024. Available online: https://www.nystator.com/col.jsp?id=112 (accessed on 17 November 2025).

42. Sun, P.; Zhang, C.; Chen, J.; Zhao, F.; Liao, Y.; Yang, G.; Chen, C. Decoupling Design and Verification of a Free-Piston Linear Generator. *Energies* **2016**, *9*, 1067. [CrossRef]
43. Bassett, M.; Thatcher, I.; Bisordi, A.; Hall, J.; Fraser, N.; Warth, M. Design of a Dedicated Range Extender Engine. In Proceedings of the SAE Technical Paper 2011-01-0862, SAE 2011 World Congress & Exhibition, Detroit, MI, USA, 12 April 2011. [CrossRef]
44. Verhelst, S.; Wallner, T. Hydrogen-fueled Internal Combustion Engines. *Prog. Energy Combust. Sci.* **2009**, *35*, 490–527. [CrossRef]
45. European Parliament and Council of the European Union. *Regulation (EC) No 715/2007 on Type Approval of Motor Vehicles with Respect to Emissions from Light Passenger and Commercial Vehicles (Euro 5 and Euro 6)*; Publications Office of the European Union: Luxembourg, 2007.
46. European Commission. *Commission Regulation (EU) 2017/1151 Supplementing Regulation (EC) No 715/2007 with Respect to Emissions from Light Passenger and Commercial Vehicles*; Publications Office of the European Union: Luxembourg, 2017.
47. Mattia Marega. Comparative LCA Assessment of Diesel Oil and Hydrogen Internal Combustion Engines for Power Generation. Master's Thesis, Politecnico di Torino, Torino, Italy, 2024.
48. Mainspring Energy. Linear Generator (LGen) Technology. Available online: https://www.mainspringenergy.com/product (accessed on 18 July 2025).
49. WB Power Services. Technical Specification: Agenitor 412 Pure H2 | ct0-0 Technical Report Doc.-ID 2348713, Rev. M, WB Power Services. 2021. Available online: https://www.wbpsltd.co.uk/wp-content/uploads/2023/08/TSP_agenitor-412-Hydrogen50Hz400V__2678133.pdf (accessed on 4 November 2025).
50. Changsha Mingbang Intelligent Technology Co., Ltd. ISO 9001 Certified 400KVA Diesel Generator Set with 400V/230V and 50Hz/60Hz Frequency. Available online: https://www.dieselgen-sets.com/sale-54136521-iso-9001-certified-400kva-cummins-diesel-generator-set-with-400v-230v-and-50hz-60hz-frequency.html (accessed on 4 November 2025).
51. Candelaresi, D.; Valente, A.; Iribarren, D.; Dufour, J.; Spazzafumo, G. Comparative life cycle assessment of hydrogen-fuelled passenger cars. *Int. J. Hydrogen Energy* **2021**, *46*, 35961–35973. [CrossRef]
52. Benton, K.; Yang, X.; Wang, Z. Life cycle energy assessment of a standby diesel generator set. *J. Clean. Prod.* **2017**, *149*, 265–274. [CrossRef]
53. Rinawati, D.I.; Keeley, A.R.; Takeda, S.; Managi, S. Life-cycle assessment of hydrogen utilization in power generation: A systematic review of technological and methodological choices. *Front. Sustain.* **2022**, *3*, 920876. [CrossRef]

https://doi.org/10.3390/en19184360